

The Meson Production Targets in the high energy beamline of HIPA at PSI

D. Kiselev^{1*}, P. A. Duperrex¹, S. Jollet¹, S. Joray¹, D. Laube¹, D. Reggiani¹,
R. Sobbia¹, V. Talanov¹

¹ Paul Scherrer Institut, 5232 Villigen PSI, Switzerland

* Daniela.Kiselev@psi.ch

April 15, 2021



Review of Particle Physics at PSI
doi:[10.21468/SciPostPhysProc.2](https://doi.org/10.21468/SciPostPhysProc.2)

1

2 Abstract

3 Two target stations in the 590 MeV proton beamline of the High Intensity Proton Ac-
4 celerator (HIPA) at the Paul Scherrer Institut (PSI) produce pions and muons for seven
5 secondary beamlines, leading to several experimental stations. The two target stations
6 are 18 m apart. Target M is a graphite target with an effective thickness of 5 mm, Target E
7 is a graphite wheel with a thickness of 40 mm or 60 mm. Due to the spreading of the
8 beam in the thick target, a high power collimator system is needed to shape the beam
9 for further transport. The beam is then transported to either the SINQ target, a neutron
10 spallation source, or stopped in the beam dump, where about 450 kW beam power is
11 dissipated. In the following, the targets, collimators and beam dumps are further de-
12 scribed.

13 3.1 Introduction

14 The High Intensity Proton Accelerator (HIPA) at PSI [1] delivers a 590 MeV continuous proton
15 beam of up to 2.4 mA, which is accelerated in three stages and described in Section 2 [2] of
16 this review. After the last stage of the Ring cyclotron, the proton beam is sent to the two
17 meson production target stations, M and E [3]. As the Meson Production Target stations have
18 to provide good transmission to the SINQ spallation target, losses due to multiple scattering
19 and nuclear reactions in the targets have to be kept low while keeping the pion/muon yield
20 high. A low Z material is the best target choice according to [4]. In the 1980's, beryllium was
21 used, which failed after a short time at above 120 μA due to bending stresses on the location
22 of a crack [5]. Since the 1990's graphite has been used for both targets. They last for several
23 years or up to about 40 Ah of proton beam. With a 40-mm (60-mm)-thick target E, the beam
24 transmission is about 70 %, (60 %). About 10 % of the beam is scattered out of the target.
25 For further transport the beam is shaped by a collimator system, where a large fraction of the
26 beam is stopped. Targets, collimators, beam dumps and their environment have to be cooled
27 to dissipate the heat produced. Due to nuclear reactions this area is highly radioactive and
28 needs to be well shielded. Therefore measures for maintenance have to be considered and
29 provided.

30 3.2 Meson Production Target Stations

31 Pions are mainly produced by nuclear reactions of the 590 MeV protons with the nucleons
32 in the target above a threshold of about 280 MeV in the center-of-mass frame. Muons are

33 produced by pion decay. When a pion is stopped within 1 mm from the surface of the target,
34 positive muons can escape. These are called surface muons and are used for particle as well as
35 solid-state physics experiments, e.g. the examination of the magnetic properties of materials.
36 Surface muons have energies below 4.1 MeV (corresponding to 29.8 MeV/c) and are almost
37 100% polarized. Pions exiting the target can produce muons by decay in flight with much
38 higher energies, up to 60 MeV. These are called cloud muons and can have positive or negative
39 charge, although the negative charge is suppressed by a one order of magnitude.

40 Target M feeds two beamlines in the forward direction called PiM1 and PiM3. Target E
41 provides secondary particles for five beamlines, two in forward direction, PiE1 and MuE1,
42 two perpendicular to the proton beamline, MuE4 and PiE3, and one (PiE5) at a backward
43 angle. Muon and pion rates are given in Section 2 [2]. Each target is a 40-cm-diameter
44 graphite wheel that rotates at 1 Hz to distribute the heat spot from the pencil beam. Standard
45 pyrolytic graphite failed due to thermal stress as the expansion coefficients differ strongly in
46 the axial and lateral directions. Radiation induced swelling might have also played a role.
47 Thus polycrystalline graphite from SGL Carbon company is used. It consists of small single
48 crystallites of 10 to 20 μm , which are irregularly arranged in space. Therefore, the physical
49 properties are almost isotropic, as small grain sizes further improve the isotropy.

50 3.2.1 Target station E

51 20 (30) kW/mA of power is deposited by the beam in the 40 mm (60 mm) thick target E. At an
52 operating temperature of about 1700 K at 2 mA, the target is cooled primarily by radiation due
53 to the large emissivity of graphite. Water-cooled copper shields are mounted on the rear of the
54 target within the vacuum chamber to dissipate the heat. As the target is mainly surface cooled,
55 the maximum temperature is approximately independent of the target thickness. However,
56 since the beam losses are higher with the 60 mm target, the maximum beam current for a
57 60-mm thick target is limited to 2 mA due to cooling issues.



Figure 3.1: Left: Exchange flask (yellow) for the Target E insert. In the background in orange is the exchange flask of Target M. Right: Target E insert with the old graphite wheel design.

58 The target with its shielding plug (Figure 3.1 right) is inserted vertically into the beamline.
59 As a consequence, the horizontal rotating shaft has to be small and so the two bearings must
60 be close to the target. For this reason, heat transfer to the bearings has to be reduced by proper
61 target design. For this, the graphite and the hub with the bearings are connected by only six
62 hollow spokes, which maintain the target shape but can also follow dimensional changes due
63 to thermal expansion. After 2002, the graphite rim has been separated into 12 segments by
64 slits of 1 mm to reduce deformation of the rim (Figure 3.2 left). Before, the radial deformation

3.2 Meson Production Target Stations

65 of the graphite wheel was observed to increase with rising beam current. This could cause the
66 proton beam to partly miss the target as its width is just 6 mm. The small width favours surface
67 muons from the produced pion distribution, which roughly follows the beam shape. It also
68 keeps the temperature gradient between the center and the surface of the target small, which
69 reduces thermal stress. However, it requires that the proton beam is always well centered.
70 This is accomplished by a beam centering system relying on the beam position monitors in
71 front of the target stations. Further, the transmission of the beam is controlled constantly and
72 a deviation leads to a beam interlock as a pencil like beam missing the target could damage
73 the SINQ target.

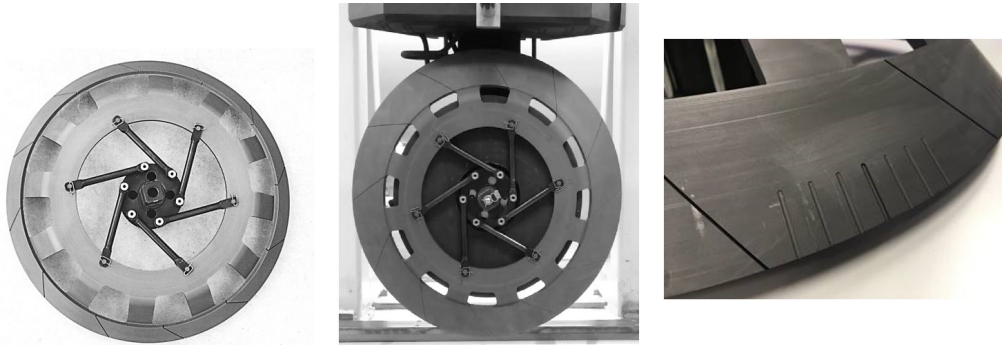


Figure 3.2: Different Target E types from 2002 on. Left: Graphite wheel with 12 segments. Middle: Slanted target type. Right: Target E with grooves.

74 Recently, the sensitivity to deviations of the beam from the center of the target was sig-
75 nificantly improved with a modified version of the graphite wheel. For this, small grooves on
76 both sides of the graphite target were applied (see Figure 3.2 right). In this way, the beam
77 transmitted through the target is modulated, when it deviates more than 0.5 mm from the
78 target centre. From there on, the amplitude of the modulation depends strongly on the posi-
79 tion of the beam. Since different spacings are used between the grooves inside and outside, a
80 deviation left and right from the center can be identified. More details, including information
81 about the Fast Fourier Transformation used for the signal analysis, can be found in [6].

82 As the bearings degrade from heat and radiation, they have to be replaced after a few
83 months of operation. First, several meters of concrete have to be removed from beamline.
84 Then the target insert with the shielding plug is pulled into the exchange flask by remote
85 control. The 42-t exchange flask (Figure 3.1 left) is well shielded by up to 40 cm steel for the
86 up to 3 Sv/h graphite wheel [7]. The same shielding flask is used for removing collimators
87 and beam dumps out of the beamline. The exchange flask is transported with the 60 t crane
88 to a door lock above the service cell (ATEC) at PSI. The door lock is remotely opened by the
89 control unit of the exchange flask. Then the target insert is lowered into the service cell,
90 which is equipped with manipulators for remote handling. The hub with the two bearings
91 are exchanged using these manipulators. During scheduled user beam time, the second target
92 insert, which is fully equipped and has been stored in a vacuum chamber, is put back into the
93 beamline to reduce the downtime.

94 A new type of target wheel was successfully tested at the end of 2019. Unlike the standard
95 wheel, the beam here passes with a small angle through the graphite, keeping the effective
96 target thickness (40 mm) the same (see Figure 3.2 middle). This configuration, called slanted
97 target, results in a larger active surface and has two locations, the entrance and exit of the
98 beam, where the beam is close to the surface. Both effects lead to an increase of surface
99 muons. A first analysis [8] indicates an increase of 40 - 50 %.

100 **3.2.2 Target station M**

101 As the Target M has a much smaller thickness, and the bearings are far from the beam and
 102 placed in the shielding, the demands are much less challenging than for Target E. The rim
 103 of the target is about 2-cm wide with a thickness of 2 mm. As the beam passes through the
 104 rim at an angle of 30° , its effective thickness is 5.2 mm (see Figure 3.3 left). This leads to a
 105 beam loss of only about 1.6 % in the target and the following collimator system. The power
 106 deposition is about 2.4 kW/mA and the target operates at around 1100 K, mainly cooled by
 107 thermal conduction.

108 The original design dates back to 1985. The 85-cm steel shielding plug is placed upstream
 109 of the target and is not accessible during beam operation. The target insert is mounted hor-
 110 izontally, which has the advantage that the rotating shaft is long and the two bearings are
 111 well shielded. This results in bearing lifetimes of several years. In 2012/13 a new target in-
 112 sert was designed and installed in the beamline (see Figure 3.3 right). The bearing lifetime
 113 is improved due to better cooling of the front of the shielding plug close to target and beam.
 114 Here an additional copper plate cooled by water, is attached. The rotating shaft is made of
 115 low conducting material, titanium-vanadium, to reduce the heat flux from the target to the
 116 bearings. In this design the bearings can be exchanged without changing the target by pulling
 117 the shaft through the shielding plug. Further improvements in the maintenance and handling
 118 of the vacuum seal at the rear of the target insert were implemented in the new design.

119 In the near future, precision particle physics experiments will require higher rates, particu-
 120 larly for surface muons, to stay at the forefront of muon intensity. HIMB, High Intensity Muon
 121 Beam, aims to increase the surface muon rate with a 20-mm thick slanted target design and
 122 beamlines transporting a large fraction of the secondary particles produced. An increase of
 123 two orders of magnitude in the rates for surface muons is envisaged.

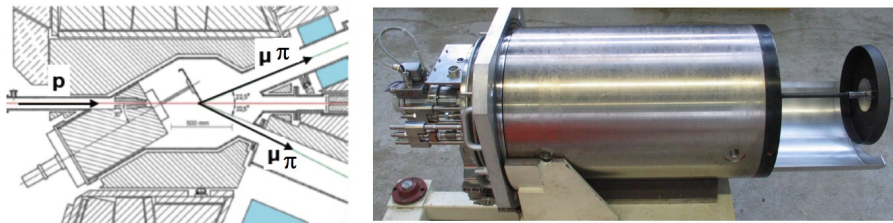


Figure 3.3: Left: Schematic view of the Target M insert at the beamline. Right: The Target M insert, new design.

124 **3.3 High Energy Collimators and Beam dump**

125 As the collimators and beam dumps have to stand high power from the proton beam, both
 126 devices are similar in their design. Like Target E, they are inserted vertically and contain steel
 127 shielding above the component. Collimators and beam dumps are both made from oxygen-
 128 free, high purity copper for three reasons: to have good thermal conductivity, to avoid hy-
 129 drogen embrittlement and for brazing of the steel tubes onto the copper body. Hydrogen
 130 embrittlement occurs at high temperatures and can lead to cracks. The hydrogen is not an
 131 impurity in the copper but produced by spallation reactions of the protons with copper. Hy-
 132 drogen bonds to the oxygen present in copper as impurity to form water, which then causes
 133 cracks at elevated temperatures. Brazing requires an oxygen-free surface. However, during
 134 brazing at temperatures around 800°C oxygen diffuses out of the copper and passivates the
 135 surface leading to a bad junction and thermal contact.

136 Cooling is quite important to avoid not only melting but temperatures above the homol-
 137 ogous temperature (half of the melting temperature in Kelvin), where the structure of the
 138 material starts to change significantly. Therefore, temperatures above 400°C in copper must
 139 be avoided. Since direct contact of the water with the proton beam is not recommended due
 140 to the production of aggressive ions that lead to corrosion, the water pipes are wound out-
 141 side of the cylindrical body. With a water flux of about 8 m/s the tubes cannot be made from
 142 copper, since they would suffer from abrasion, which leads to erosion corrosion. Therefore
 143 steel tubes are brazed to the copper body, which requires a good thermal contact in between.
 144 Before a new device is put into the beamline, the thermal contact is tested by heat exchange
 experiments.

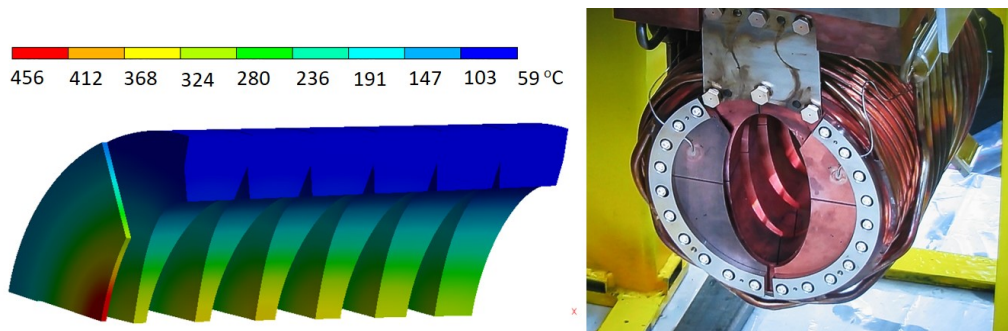


Figure 3.4: Left: Temperature distribution of the KHE2 with 2 mA beam. Right: Collimator KHE2 with sample plate from the backside.

145 The cylindrical copper body is composed of five or six slices, which are later brazed to-
 146 gether. This shape cannot be manufactured from one block, since some of the slices are tai-
 147 lored on both sides to reduce the energy deposit of the proton beam by reducing the amount
 148 of material. Slits between the slices also help to reduce the thermal stress. Each slice also
 149 contains four radial slits for thermal expansion. The optimal shape of the collimator has to
 150 be found by computational fluid dynamics (CFD) or equivalent simulations, which take into
 151 account the actual distribution of the proton beam or import the energy deposition region-
 152 wise from particle transport Monte Carlo simulations. The temperature distribution inside the
 153 collimator KHE2 along the beam direction is shown in Figure 3.4 left. More than one device
 154 is often necessary to absorb the beam under the constraint that the maximum temperature is
 155 kept below the homologous temperature and that the device still fits in the exchange flask.
 156 In fact, the collimator system and the beam dump each consist of four parts. The maximum
 157 length of each part is 400 mm. The collimator system after Target E is distributed along 4
 158 m, whereas the beam dump sections are separated from each other by about 100 mm. An
 159 aperture, separated in four sectors, is mounted in front of most devices. It consists of 100 μm
 160 Nickel foil, where free electrons from ionization due to protons are collected. This signal is
 161 proportional to the fraction of the beam in a section, and serves as an indication of the beam
 162 position as well as the beam size. The aperture is used to protect the device behind with a
 163 machine interlock, if the beam properties deviate from normal.

165 The KHE2, the third collimator after Target E, absorbs between 100 kW and 140 kW of
 166 the beam depending on the beam tuning and the thickness of Target E. This means that a
 167 large fraction of the beam hits the collimator and might cause radiation damage. An early
 168 estimate using the particle transport Monte Carlo package MCNPX2.5.0 [9] predicted an av-
 169 erage DPA (Displacements Per Atom) of around 20. Regions close to the beam have an up
 170 to four times higher DPA value. Therefore, visible signs of radiation damage were expected
 171 and the collimator was inspected in the hot and service cell ATEC of PSI. The inside of the

3.4 Summary

172 collimator was examined by an inspection tool to avoid high doses to the camera [10], which
173 was well shielded without direct view to the collimator. This was necessary due to a dose rate
174 of 310 Sv/h, 10 cm from the entrance of the collimator. No cracks or serious damage were
175 observed except for some pieces peeling off the collimator. These pieces were identified as
176 graphite (by the grey color) as well as due to the presence of ^7Be , a typical radioisotope from
177 carbon activation. The graphite likely sublimated from Target E. A sample was taken and later
178 a measurement with a HPGe (High Purity Germanium) detector was performed. In addition,
179 traces from the brazing material, such as silver isotopes, were found. In 2013 the KHE2 was
180 replaced by a new collimator of identical design, but with more thermocouples and additional
181 sample plates from copper and Glidcop, a copper matrix with 0.3 wt % aluminum oxide, for
182 later material studies after irradiation (See Figure 3.4 right). Glidcop is a promising candi-
183 date with similar properties as copper but keeping a large fraction of the thermal conductivity
184 under irradiation.

185 In the meantime a new collimator system KHE2 and KHE3 with a different inner shape
186 was manufactured, which will stand up to 3 mA beam current. The maximum current for the
187 present KHE2 is 2.15 mA according to CFD simulations, which use the physical and mechanical
188 properties for unirradiated copper. The main difference in the design is that the inner cone of
189 the present collimator KHE2 has a diameter that widens in beam direction, whereas in the new
190 design it decreases as in the beam dumps. Therefore, on the slices in front of the new designed
191 KHE2 much less beam power is absorbed as the cone opening at this position is much wider.
192 A side effect is that the slices are only slightly tailored. With the new design beam transport
193 with a 3% larger transmission is possible up to the SINQ target.

194 In 2016 a sudden increase of the vacuum pressure inside the beam tube in the vicinity of
195 the beam dump indicated a malfunctioning component. However, it was not clear which com-
196 ponent was causing the problem. A mass spectrometer connected to the beam tube indicated
197 the presence of water, which restricted the leak to a component cooled by water. However,
198 there are many components, such as slits, vacuum chambers and beam dumps, connected to
199 the cooling water cycle. The leak appeared at a beam current above 1.4 mA measured in front
200 of the 40-mm Target E. However, it was very difficult to locate the leak, since it could not be
201 detected without beam, and also did not show up when the device was heated with 150 °C
202 pressurized water. Since the full beam dump consists of four parts, the malfunctioning part had
203 to be identified before a replacement could be manufactured. The leak was identified with
204 beam studies, and finally confirmed when the leak disappeared in 2018 with a new identical
205 BHE1 in place. During the time the first beam dump section was removed from the beam-
206 line and transferred to ATEC for inspection and replacement, a periscope using mirrors was
207 inserted into the beamline at the position of BHE1. A camera at its end took pictures from
208 the second part of the beam dump as well as the entry of the vacuum chamber. A view on the
209 BHE2 from this camera is shown in Figure 3.5 left. On the right of the figure, BHE2 is shown
210 before irradiation. As can be seen from the pictures BHE1 is intact despite withstanding 150
211 kW with beam.

212 3.4 Summary

213 The two meson production stations M and E use rotating polycrystalline graphite targets. They
214 have been working well since the 1990's, serving seven beamlines with pions and muons. A
215 special target design with grooves was recently tested and allows a very precise detection of
216 the beam position on the target. For HIMB aiming to increase the surface muon rate by up to
217 a factor of 100, beamline simulation and design studies for an upgrade of the target M station
218 with the new type of slanted target design are ongoing. In the Target E station the slanted
219 target type already demonstrated a 40-50% increase of the surface muon rate.

220 The collimator system as well as the beam dump have to stand more than 100 kW per

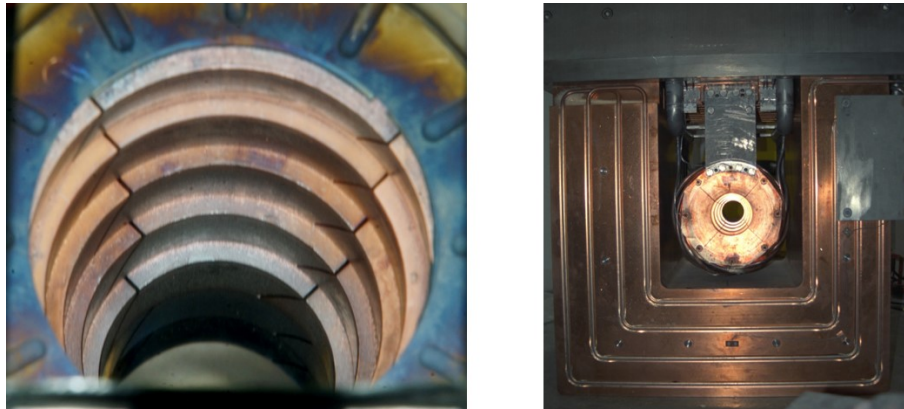


Figure 3.5: Left: Beam dump BHE2 with aperture in the beamline as seen from the periscope. Right: BHE2 without aperture before irradiation in 1990.

221 component. Except for a water leak in the first beam dump element, which is likely due
222 to thermal cyclic stress, no visible signs of radiation damage are observed. The design of a
223 segmented copper body cooled by water in steel tubes, which are brazed to the copper, has
224 proven its reliability.

225 Acknowledgment

226 We would like to thank Pedro Baumann for the excellent maintenance and further improve-
227 ment of the target and beamline components. Further we thank Thomas Rauber for taking
228 care of the secondary beamlines and for the inspection of the beam dump region with the
229 periscope. Finally we thank the many specialized technical groups for supporting the 590
230 MeV beamline and target region at HIPA.

231 References

- 232 [1] D. Kiselev, C. Baumgarten, R. Dölling, P. Duperrex, D. Götz, J. Grillenberger, D. Reggiani,
233 M. Schneider, M. Schippers, M. Seidel and H. Zhang, *Status and Future Projects of the*
234 *PSI High Intensity Proton Accelerator*, doi:[10.7566/JPSCP.33.011004](https://doi.org/10.7566/JPSCP.33.011004).
- 235 [2] J. Grillenberger and et al., *The High Intensity Proton Accelerator at PSI*, *SciPost Phys.*
236 *Proc.* **2**, ppp (2021), doi:[10.21468/SciPostPhysProc.2.XXX](https://doi.org/10.21468/SciPostPhysProc.2.XXX).
- 237 [3] D. Kiselev, P. Baumann, P. Duperrex, S. Jollet, P.-R. Kettle, A. Knecht, D. Laube, C. Nyfeler,
238 A. Papa, D. Reggiani, R. Sobbia, V. Talanov *et al.*, *Progress and Challenges of the PSI*
239 *Meson Targets and Relevant Systems*, doi:[10.7566/JPSCP.33.011102](https://doi.org/10.7566/JPSCP.33.011102), <https://journals.jps.jp/doi/pdf/10.7566/JPSCP.33.011102>.
- 241 [4] F. Berg *et al.*, *Target studies for surface muon production*, *Phys. Rev. Acc. & Beams* **19**,
242 024701 (2016), doi:[10.1103/PhysRevAccelBeams.19.024701](https://doi.org/10.1103/PhysRevAccelBeams.19.024701).
- 243 [5] G. Heidenreich, *Carbon and beryllium targets at psi*, In W. Chou, ed., *Proc. 20th Interna-*
244 *tional Workshop of High Intensity and High Brightness Hadron Beams*, p. 122. American
245 Inst. of Physics, Batavia, Illinois (2002).
- 246 [6] P.-A. Duperrex, P. Baumann, S. Joray, D. Kiselev, D. Laube and D. Reggiani, *New Cen-*
247 *tering Beam Monitor for High Power Proton Beam Rotating Target*, In *Proc. Cyclotrons'19*,

- 248 no. 22 in International Conference on Cyclotrons and their Applications, pp. 189–191. JA-
249 CoW Publishing, Geneva, Switzerland, ISBN 978-3-95450-205-9, doi:[10.18429/JACoW-](https://doi.org/10.18429/JACoW-Cyclotrons2019-TUP016)
250 [Cyclotrons2019-TUP016](https://doi.org/10.18429/JACoW-Cyclotrons2019-TUP016) (2020).
- 251 [7] D. Kiselev, R. Bergmann, D. Schumann, V. Talanov and M. Wohlmuther, *Proton induced*
252 *activity in graphite - comparison between measurement and simulation*, J. Phys. **1046**,
253 1203 (2018).
- 254 [8] P.-R. Kettle, Private communication.
- 255 [9] *Mcnpx user's manual, version 2.5.0*, LA-CP-05-0369 (2005).
- 256 [10] A. Strinning, P. Baumann, M. Gandel, D. Kiselev, Y. Lee and S. Adam, *Visual inspection of*
257 *a copper collimator irradiated by 590 mev protons at psi*, In *Proc. 46th International Work-*
258 *shop of High Intensity and High Brightness Hadron Beams*, p. 245. Morschach, Switzerland
259 (2010).